Raman Spectroscopy of Nanoparticles Using Hollow-Core Photonic Crystal Fibers

Juan Irizar, *Student Member, IEEE*, Jordan Dinglasan, Jane Betty Goh, Altaf Khetani, Hanan Anis, Darren Anderson, Cynthia Goh, and A. S. Helmy, *Senior Member, IEEE*

(Invited Paper)

***Abstract*—Hollow-core photonic crystal fibers (HC-PCF) were employed for enhancing the Raman signal obtained from ZnO nanoparticles (NPs) in solution. By selectively filling the core of HC-PCF, substantial enhancement in the Raman signal was obtained. By employing this technique, four different stages in the synthesis ZnO NPs were studied with record low pump power levels. The concentration of ZnO NPs in the system was $<1\%$ by weight of the total mass. Yet, the different synthesis stages could be differentiated and identified through the Raman modes obtained. It was also demonstrated that the concentration of NPs in solution could be obtained with sensitivity in the millimolar range. This could be achieved by examining the amplitude ratios of the relevant Raman modes.**

***Index Terms*—Colloidal nanoparticles (NPs), photonic crystal fibers (PCFs), Raman enhancement, Raman spectroscopy, ZnO nanoparticles.**

I. Introduction

COLLOIDAL nanoparticles (NPs) have emerged over the last decade as promising candidates for novel optical electronic, and magnetic materials [1]. NPs are aggregates of a few hundred to tens of thousands of atoms. They are commonly manufactured through wet chemistry processes in which the solvent accounts for more than 99% of the weight of the entire system [2]. Usually NPs are stabilized using surfactants or polymer stabilizers to prevent their agglomeration during use and synthesis. With a diameter in the nanometer range, NPs are larger than individual atoms but smaller than bulk solids. Therefore, they exhibit physical and chemical properties that fall in between their bulk and atomic counterparts [1]. NPs offer material developers the ability to tune the novel properties which NPs can provide by changing their size, composition, or capping layer. This renders their optical, electronic, and magnetic properties sufficiently flexible to be adapted to a wide range of applications.

The potential of NPs as promising optoelectronic materials is progressively being demonstrated in the literature [1], [3], [4]. There has also been an increasing interest in their use for biomedical applications including medical drug targeting, contrast agents for *in vivo* imaging, and targeted fluorescent labels [5], [6]. In addition, NPs have been shown to serve as excellent candidates for chemical catalysts [7], [8]. For this wide range of applications to be attainable using NPs, stringent optimization is required to tailor their properties to suit each application. *In situ* monitoring of their synthesis is challenging because of the solution-based environment in which NPs are produced. Also, the solution-based environment entails that techniques developed for *in situ* characterization of other nanostructures, such as epitaxially grown quantum wells, wires, and dots are often not suitable.

Molecular beam epitaxy (MBE), for example, provides atomic-level control over epitaxial layer growth. Perfecting the growth of quantum wells, wires, and dots using MBE was achieved owing to *in situ* monitoring techniques, such as reflection high-energy electron diffraction (RHEED), which played a pivotal role in developing the precision of the epitaxial growth technologies available today [9]. Similar techniques are required to monitor solution-based NPs syntheses to improve control over NPs size, composition, and construction of complex structures.

Several techniques have been employed to characterize NPs after their fabrication [10], [11]. The most common techniques include: photoluminescence (PL) and absorption spectroscopy, Mie scattering, transmission electron microscopy (TEM), SEM, and X-ray diffraction. The complementary use of these techniques has provided valuable information about the behavior and characteristics of NPs, after fabrication. However, unlike other nanostructures, there has been little effort in studying NPs growth dynamics *in situ*. This can be ascribed to two factors. First, the low NPs concentration during fabrication imposes difficulties in retrieving strong spectroscopic signals. In addition, commonly used characterization techniques, with PL being an excellent example, are insensitive to many NPs precursors [12].

Raman spectroscopy is an optical, noninvasive technique that probes vibrational modes of matter [13]. It has been exploited to study a wide range of nanostructures including epitaxial quantum wells, wires and dots, superlattice structures,

Manuscript received September 21, 2007; revised March 17, 2008. This work was supported in part by the National Science and Engineering Research Council, Canada, under Discovery Grant 293258/5.

J. Irizar and A. S. Helmy are with Edward S. Rogers Sr. Department of Electrical and Computer Engineering, Institute of Optical Sciences, University of Toronto, Toronto ON M5S 1A7, Canada (e-mail: juan.irizar@gmail.com; a.helmy@utoronto.ca).

J. Dinglasan, J. B. Goh, and D. Anderson are with Northern Nanotechnologies, Toronto ON M5S 1A7, Canada (e-mail: jdinglasan@nntech.com; jgoh@chem.utoronto.ca; danderson@nntech.com).

A. Khetani and H. Anis are with the School of Information Technology and Engineering, University of Ottawa, Ottawa ON K1N 6N5, Canada (e-mail: altafkhetani@gmail.com; hanan@site.uottawa.ca).

C. Goh is with the Department of Chemistry, Institute of Optical Sciences, University of Toronto, Toronto ON M5S 1A7, Canada (e-mail: cgoh@chem.utoronto.ca).

Color versions of one or more of the figures in this paper are available online at http://ieeexplore.ieee.org.

Digital Object Identifier 10.1109/JSTQE.2008.922915

and nanotubes [14], [15]. Nevertheless, characterization of NPs in their native and dilute aqueous environment using Raman scattering has not received significant attention. This is chiefly due to the weak Raman signals obtained from such aqueous systems.

This paper proposes and demonstrates the use of Raman spectroscopy as a probe for monitoring NPs growth. A hollow-core photonic crystal fiber (HC-PCF) is used as a means of enhancing the Raman signal from the NPs constituents. The system studied consists of ZnO NPs capped with polyacrylic acid (PAA) dispersed in distilled water. This paper is organized as follows. Section II discusses enhancement techniques used to improve Raman signal to noise ratio. Section III discusses HC-PCF as an alternative enhancement technique for Raman spectroscopy. It is then shown how HC-PCF can serve as an optimum candidate for *in situ* monitoring of NPs growth. Section IV presents a Raman study of different synthesis stages of ZnO NPs. Conclusions are discussed in Section V.

II. Raman Spectroscopy Enhancement Techniques

Raman spectroscopy probes lattice vibrations, which are sensitive to the local environment in which the probed atoms are located [13]. Therefore, changes in the Raman modes wavenumbers, peak widths, or relative strengths with respect to other modes can indicate variations in lattice order, stress distribution, temperature, or chemical composition. Furthermore, quantum-confined heterostructures, such as NPs have unique phonon modes, which arise due to the quantum confinement [15].

Spontaneous Raman spectroscopy, the most widely used type of Raman analysis, has been used since 1928 for the study of liquids [16]. Substantial pump power densities are often required to retrieve useful Raman spectra from solutions, where sufficient signal to noise ratio for mode analysis is obtained [17]. In practice, Raman signals cannot be retrieved using conventional far-field optics for solutions featuring solute to solvent mass ratios comparable to those used in NPs synthesis processes.

There exists a range of techniques that can be used to enhance Raman signals in comparison to those obtained using spontaneous Raman spectroscopy. These include surface-enhanced Raman spectroscopy (SERS) [18], [19], resonant Raman spectroscopy (RR) [20], coherent anti-Stokes Raman scattering (CARS) [21] and Raman spectroscopy within liquid core waveguides (LCW) [22], [23].

Signal enhancement in SERS is induced by silver or other metal particles. These NPs are often mixed with the sample under investigation. Raman signal enhancement is achieved thanks, mainly to the strong electric fields created by the excitation of localized and delocalized surface plasmons between the silver metallic particles and the surrounding dielectric medium. Distinct advantages of SERS include detection limits at the parts per billion level, and unparalleled specificity [19].

In RR, the energy of the incoming laser is adjusted such that either itself or the resulting scattered light coincide with an electronic transition of the molecule or sample under test. This ensures that the sample is excited near one of its electronic resonances, where the Raman cross section is at a maximum. RR provides excellent selectivity since different molecules or materials posses a unique set of electronic resonances [20].

CARS is based on a third-order nonlinear optical process. It involves two ultrafast pulsed laser beams, the pump and Stokes beams. When the difference in the frequency of both beams is in resonance with the frequency of a Raman-active molecular vibration in the sample, a strong CARS signal is produced [21]. It has recently been demonstrated as a powerful tool for noninvasive, chemical imaging of biological systems.

Raman spectroscopy within LCW has been studied since 1972 as another platform for Raman enhancement. It relies on an increase in the interaction length between the light and the liquid sample. This is achieved using total internal reflection (TIR) of the pump beam in a waveguide filled with the liquid under test in its core. Capillary tubes of several meters in length and diameters of the order of 100 μm have been used to enhance the Raman signal from different biological and inorganic solutions alike [22], [23].

The enhancement in the Raman signal provided by the aforementioned techniques range between 2 and 6 orders of magnitude. These techniques, however, do not provide an optimum platform for *in situ* monitoring of NPs synthesis. The addition of metallic NPs to the sample in SERS could influence NPs synthesis, either due to chemical incompatibility between the metal NPs and their precursors, or by altering the reaction dynamics due to the presence of additional nucleation centers. RR is restrictive as it requires the samples tested to possess electronic resonances within the wavelength range of conventional lasers. CARS involves a more elaborate setup that requires two synchronized ultrafast lasers with at least one of them tunable. Raman spectroscopy within LCW poses constraints on the refractive index of the solution under study. Given their radius, the capillary tubes used for LCW often exhibit multimode waveguiding. This provides nonuniform intensity within the LCW core, which reduces the obtained Raman signal to noise ratio.

The next section demonstrates how HC-PCFs serve as an alternative platform for enhancing Raman signals from aqueous samples.

III. Raman Spectrosocopy with HC-PCFs

In contrast to conventional optical fibers that rely on TIR, HC-PCF is a class of fibers that relies on photonic bandgap (PBGs) effects in the cladding to achieve waveguiding [24]. An HC-PCF features an air core surrounded by a nanostructured silica cladding. The latter induces a spatial modulation in the index of refraction around the core that produces PBGs in the cladding to support low-loss guided modes within the core [25], [26].

A key feature of the HC-PCF is that single-mode waveguiding over a wide range of wavelengths can be achieved with appropriate cladding design [26]. Another feature, which is pertinent to this paper is that the PBG-based waveguiding is attainable for a wide range of core refractive indices. This means that single-mode waveguiding is achievable in HC-PCF for NPs dispersed in a wide range of solvents [27], [28]. These characteristics provide key advantages for Raman spectroscopy.

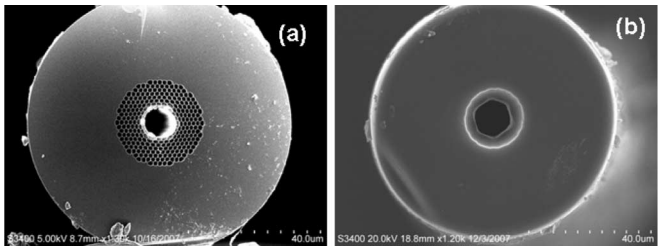

Fig. 1. (a) SEM image of the cross section of a HC-PCF. (b) SEM image of a HC-PCF with the cladding sealed using a fusion splicer.

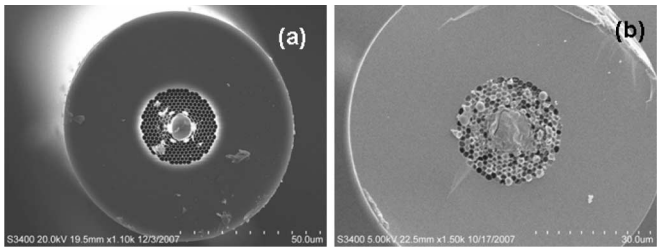

Fig. 2. (a) SEM shows an HC-PCF with the core selectively filled by submerging the end of a sealed fiber [like the one shown in Fig. 1(b)] in an optical adhesive solution. (b) SEM in HC-PCF that has been nonselectively filled by submerging an unsealed fiber [like the one shown in Fig. 1(a)] in an optical adhesive.

If the core of an HC-PCF is filled with a dilute solution of NPs, Raman scattering will be induced along the fiber's entire length. In addition, the wavelengths of the induced Raman modes will also be guided by the fiber. As a result the intensity of the Raman signal collected at a fiber's output is significantly enhanced for these Raman modes.

The use of an HC-PCF for Raman enhancement has unique advantages compared to the other enhancement techniques discussed in Section II. It does not require the addition of metallic NPs; it uses continuous wave (CW) lasers similar to those utilized for conventional spontaneous Raman spectroscopy and it may be extended to study NPs dispersed in solvents with any index of refraction.

In the rest of this section, the experimental details used in the Raman measurements using HC-PCF are described.

A. Hollow-Core Photonic Crystal Fiber

The HC-PCFs used in these experiments were obtained from Thorlabs, HC19-532. They feature an air core of 9.5 μm in diameter, surrounded by a silica microstructured cladding with an air fill fraction $>90\%$ and a diameter of 30 μm. The microstructured cladding is composed of hexagons in a triangular lattice with a pitch of 1.5 μm. The core is formed by removing 19 cells from the center of the microstructured cladding. The total diameter of the silica cladding is 90 μm, and the fiber outer diameter, including the polymer jacket, is 220 μm. The fiber has a bandgap bandwidth of 30 nm, centered at a wavelength of 535 nm. The mode field diameter is $\sim$7 μm [29].

The HC-PCF was divided into segments that were then stripped and cleaved using a conventional single-mode-fiber cleaver. An SEM of a cleaved fiber is shown in Fig. 1(a). After stripping and cleaving, the length of the fibers used for the Raman measurements was 5 cm.

B. Selective Filling of the Core

In order to selectively fill the 9.5 μm core with solution, the microstructured cladding was sealed at one of the fiber facets. Capillary effects were then used to selectively fill the core. This sealing of the microstructured cladding at one facet was achieved by treatment with a high-temperature arc fusion splicer (Fitel-S182 A). When tuned to the appropriate parameters, the arc discharge will sufficiently melt the microstructured cladding to seal it, while preserving the core. Fig. 1(b) shows an SEM image of a representative fiber facet after cladding collapse fiber. The cladding collapse extends in the longitudinal direction along the length of the fiber for $\sim$1 mm.

The physical process by which the silica holes collapse is complex, and is highly dependent on the heat transfer between the cladding and the core, on the viscosity of the melted silica, and on surface tension [30]. The temperature gradient between the fiber core and the cladding is sufficiently large to induce a faster collapse of the cladding holes compared to the collapse of the core. This, in turn, enables the cladding collapse while preserving the core.

C. Selective Core Filling Experiments

After sealing the cladding, fluid was loaded into the fiber's core by submerging the sealed end in a reservoir containing the fluid. Given the small dimensions of the core, capillary forces are strong enough to fill a 1.4 m column with water according to standard capillary theory [31]. The SEM in Fig. 2(a) shows the core of a selectively filled HC-PCF with the microstructured cladding unfilled. The filling used was an optical adhesive (Type J-91 from Summers Optical) that is curable using UV radiation. The same optical adhesive was loaded into a conventional HC-PCF without sealing the cladding. The SEM shown in Fig. 2(b) demonstrates that, in this case, capillary action fills both the core and microstructured cladding.

D. Raman System

The Raman system used is a *JY Horriba LabRam*, which includes a 532-nm frequency-doubled diode-pumped Nd:YAG laser. The beam is directed on to the sample by a holographic notch filter used as a dichroic mirror with a drop-off Stokes edge of <150 cm^{-1}. Light is coupled into the core of the fiber through a $10\times$ objective lens with a numerical aperture of 0.22. The Raman signal scattered from the NPs is collected through the same objective lens in a backscattered configuration. The signal is then directed into the spectrometer through a confocal aperture.

The spectrometer is 300 mm in length and it incorporates a 1200 g/mm grating, which provides a resolution of 2.4 cm^{-1}/pixel. The detection was carried out using a 16-bit Peltier cooled 1024×256 pixel charge-coupled device (CCD). Additionally, the system is equipped with a motorized XY stage with a resolution of 0.1 μm.

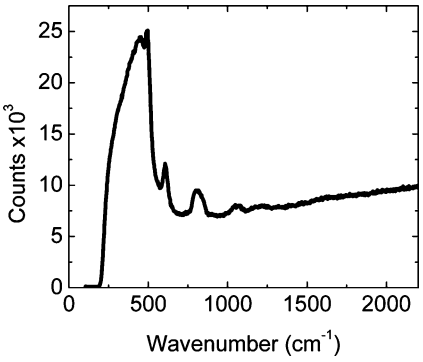

Fig. 3. Raman spectrum obtained by coupling the pump laser into an unsealed and air-filled HC-PCF. The features observed in the spectrum have been previously reported and are attributed to silica from which the fiber is made [32].

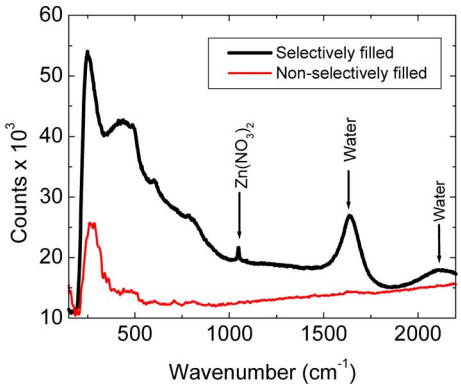

Fig. 4. Comparison of the Raman spectra obtained from a selectively filled and a nonselectively filled HC-PCF. A solution containing 99% water by weight and 1% PAA with $Zn(NO_3)_2$ was used in both cases. The features pertinent to water and $Zn(NO_3)_2$ are only evident in the selectively filled case.

E. Raman With a Selectively and Nonselectively Filled Fiber

The pump power at the output of the objective lens was 22 mW. After maximizing light coupling from the Raman system into the fiber, power out of the fiber was found to be 16 mW. The major loss in the system was attributed to the mismatch between the numerical aperture of the fiber and that of the input objective lens, which are 0.12 and 0.22, respectively. Losses due to propagation through the fiber when filled with air should account for less than 0.4 $\mathrm{dB} \cdot \mathrm{m}^{-1}$ [29].

The Raman spectrum obtained from the air-filled fiber is shown in Fig. 3. The spectrum obtained corresponds well to previous reports of the Raman signal produced in silica fibers [32].

Raman spectra from a selectively filled and a nonselectively filled fiber were first compared using dilute solution of PAA and $Zn(NO_3)_2$ ions. Fig. 4 shows the Raman spectra collected from both fibers. In the nonselectively filled case, the lack of Raman enhancement is directly attributed to shifts in the PBG away from the 532-nm laser line and the subsequent loss of waveguiding of the pump [28]. The Raman modes, which were clearly observed in the selectively filled case confirm the importance of sealing the cladding prior to loading the core with the solution under test.

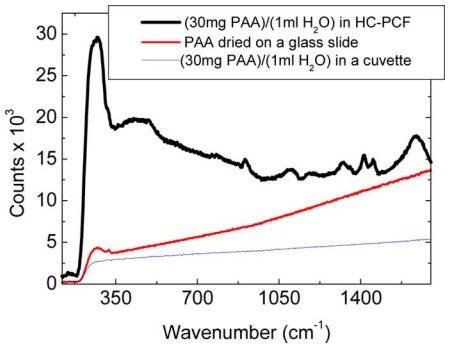

Fig. 5. Comparison of the PAA Raman spectra using different setups. Three setups used were: focusing light into an HC-PCF filled with 30 mg PAA in 1 mL of water, focusing light in a cuvette filled with 30 mg PAA in 1 mL water, and focusing light on PAA that has been dried on a glass slide. The PAA modes observed only in the case of HC-PCF are plotted in detail in Fig. 6, where the various modes identified from curve fitting are shown.

F. Raman Enhancement Obtained Using HC-PCFs

The Raman enhancement obtained using HC-PCF was investigated by comparing the Raman spectra of ZnO NPs acquired in three different conditions. In the first instance, the NPs solution was placed within a cuvette and Raman was obtained through focusing the pump laser using a 100× objective lens within the solution. The second setting tested the NPs after being dried on a glass slide with the pump laser focused using a 100× objective lens on to the dried particles. The third setting involved the NPs in solution loaded in the core of a HC-PCF with a length of 5.0 cm, as described in Section III-D. Fig. 5 shows the normalized Raman spectra for the three different cases. The water mode at 1640 cm^{-1} is only visible with the HC-PCF setup. Similarly, the modes between 500 and 1500 cm^{-1} correspond to different carbon, hydrogen, and oxygen vibrations that are only visible using the HC-PCF setup [17]. ZnO second-order Raman mode at 318 cm^{-1} was consistently observed for the liquid sample in the HC-PCF [33]. This mode was observed with a substantially reduced signal to noise ratio for the sample where NPs were dried on a glass slide.

G. Baseline Correction and Raman Mode Fitting

The Raman spectra obtained throughout this paper were analyzed in a two-step procedure. First, a baseline elimination process was carried out. This involved removing the background baseline signal using a polynomial fit. Subsequently, each Raman mode was fitted using a Lorentzian/Gaussian function with four degrees of freedom: peak amplitude, peak full-width at half-maximum (FWHM), peak shift, and a parameter determining the contributions from a Gaussian and a Lorentzian. Fig. 6 shows the accuracy of the fits obtained. Table I in the Appendix summarizes the Raman mode parameters for all the Raman modes obtained in the figures presented.

IV. Raman Investigation of ZnO Nanoparticles

Owing to their attractive properties in the UV region of the spectrum, ZnO NPs have attracted substantial attention. Applications including lasers, absorbing coatings, and photocatalysis

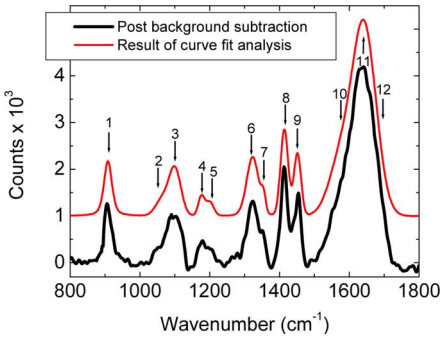

Fig. 6. Typical spectrum after the background subtraction and curve-fit analysis. The spectrum used here is that of 30 mg PAA in 1 mL of water. The curve-fit line has been offset vertically for clarity. The following modes were identified with references detailed in the Appendix. 1) Unassigned. 2) CH_2 stretch. 3) C–CH_2 stretch. 4) C–O stretch. 5) C–O stretch. 6) CH_2 twisting. 7) CH_2 twisting. 8) CH_2 deformation. 9) CH_2 deformation. 10) water. 11) water. 12) C=O stretching.

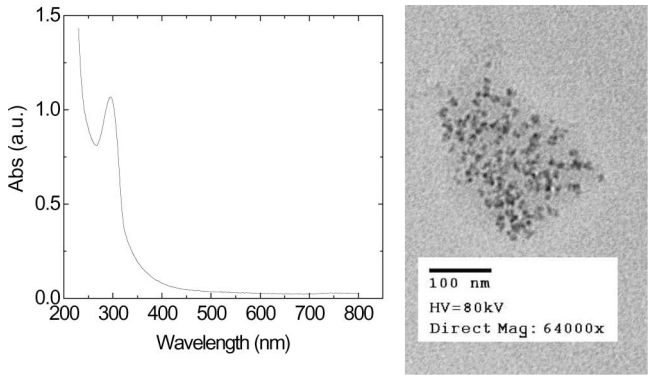

Fig. 7. UV absorption spectrum and a TEM image of purified ZnO nanoparticles.

have utilized ZnO [33]. The water-soluble ZnO NPs used in this study were prepared by the base hydrolysis of $Zn(NO_3)_2$ in the presence of PAA in water. NPs were prepared as follows. A 2 millimolar (mM) solution of $Zn(NO_3)_2$ was prepared in 1 mg/mL of 1.2×10^6 molecular weight (MW) PAA solution. The solution was then exposed to 256-nm UV light for approximately 2 h. The solution pH was then adjusted to pH 10.5 with 1 M NaOH and then was heated to 80 °C for 1 h. The solution remained clear throughout the process, which indicates that no aggregate particles of bulk ZnO was formed during the process. Formation of ZnO NPs was confirmed by the appearance of a 300-nm absorption peak and through TEM images as shown in Fig. 7. Aliquots from the reaction vessel were withdrawn at four different stages of formation of ZnO: 1) after zinc ion (Zn^{2+}) coordination with PAA; 2) after exposure to 256-nm UV light; 3) after addition of base and induction of crystallinity; and 4) after purification.

In the remainder of this section, these four stages of ZnO NPs synthesis were studied using Raman spectroscopy after being selectively filled in the core of HC-PCF.

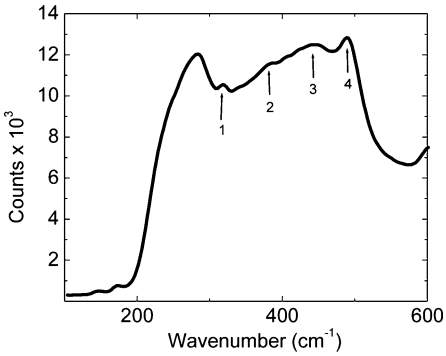

Fig. 8. Raman spectrum from HC-PCF selectively filled with a solution of 8.1×10^{-5} g of ZnO powder per milliliter of water. The mode labeled as 1) corresponds to the second-order Raman mode of ZnO. This mode is used as a reference in this study to corroborate the presence of ZnO in the nanoparticles. The modes labeled 2)–4) correspond to Raman modes from the HC-PCFs silica. A list of modes is given in the Appendix.

A. *Bulk ZnO in Solution and Water*

Distilled water and ZnO powder dissolved in distilled water were both studied separately using Raman spectroscopy in HC-PCF to serve as reference signals. Knowledge of the Raman spectra of ZnO powder in solution will aid in verifying that NPs have active ZnO. Additionally, water is the solvent for all the NPs growth stages studied in this paper and it is therefore a common background signal.

The ZnO powder was prepared by adding 0.5 mL of 2 mM $Zn(NO_3)_2$ to 0.5 mL of 13.5 mM of NaOH. The resulting solution was vortexed and then heated to 80 °C for 30 min in a water bath. White powder, corresponding to ZnO precipitated after heating. The powder was then redissolved in distilled water resulting in a solution that had approximately 8.1×10^{-5} g of ZnO per mL of water. This suspension was used in the measurements without further purification. Fig. 8 shows the Raman spectrum of this solution. The fast drop of the spectrum at $\sim$200 cm^{-1} is due to the Raman notch filter cutoff. The Raman mode at 318 cm^{-1} is attributed to a second-order ZnO Raman mode in which two-photon absorption is responsible for the production of a phonon [33]. The significant background signal from the HC-PCF between 300 and 500 cm^{-1} poses a serious drawback in the study of ZnO since it overlaps with its LO and transverse (TO) optical Raman modes [33].

Fig. 9 shows the spectrum of water up to 5000 cm^{-1}. Three features are observed: a bending O–H mode (υ_2 mode) centered at 1640 cm^{-1}, and two O–H stretching modes at 3234 and 3419 cm^{-1}, respectively, (υ_1 and υ_3) [34]. In addition, features centered at 2094 and 3963 cm^{-1} were observed. These have been attributed to OH vibrations and an associated overtone, respectively, in previous studies [34].

B. *Step 1: Zinc Ion (Zn^{2+}) Coordination With PAA*

The first step in the synthesis of ZnO NPs is the addition of $Zn(NO_3)_2$ to PAA. The addition of $Zn(NO_3)_2$ brings a noticeable change in the Raman spectra, where a Raman mode at 1047 cm^{-1} appears as shown in Fig. 10. This mode arises from the NO_3 species, as observed and reported previously [35]. To

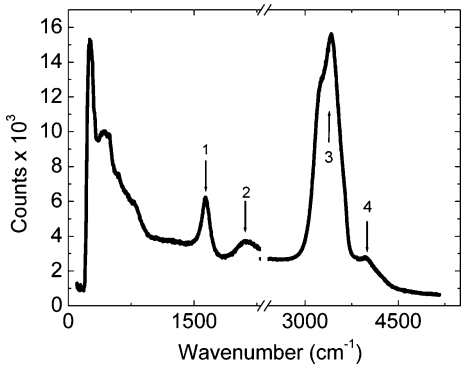

Fig. 9. Raman spectrum of distilled water obtained using an HC-PCF. The modes identified from the spectrum. 1) OH bending. 2) OH vibrations. 3) OH stretching. 4) OH overtone. A list of modes is given in the Appendix.

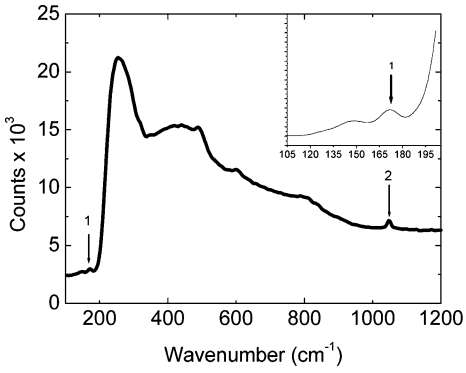

Fig. 10. Raman spectrum obtained using an HC-PCF of 99% water by weight with PAA after the addition of $Zn(NO_3)_2$ in a key step in the manufacturing process. The inset shows a detail of the Raman mode 1). The two modes observed correspond to 1) complex of Zn with NO_3 at 173 cm^{-1}, 2) symmetric stretching of NO_3 at 1049 cm^{-1}. A list of modes is given in the Appendix.

confirm the relation of this mode to the NO_3 species, an experiment was carried out on a solution of $NaNO_3$ in PAA. Raman spectroscopy of a solution containing $NaNO_3$ and PAA resulted in the appearance of the same Raman mode implying that this mode is uniquely dependent on the NO_3 species. The NO_3 in solution are merely spectator ions in the manufacturing process and they can be considered an impurity to the system.

Shifts in the C=O modes of the polymer that are located at $\sim$1700 cm^{-1} often serve as a sensitive probe to detect changes in the polymer's surrounding environment. A reduction in wavenumber of the C=O modes is usually observed as the C=O coordinates with metal ions and/or when bonds to surfaces are created [36]. This cannot be seen in the spectra shown in Fig. 10, however. This is because OH bending modes of water are much stronger than the weaker polymeric C=O modes, preventing their observation.

C. Step 2: Exposure to 256-nm UV Light

After the addition of the metal cation Zn^{2+}, the solution is then exposed to 254-nm UV light to facilitate the stabilization of the ZnO NPs. The effects of UV-irradiation cannot be easily discerned at the low concentrations used. By further concentrating the solution ten times, it was possible to observe changes in the

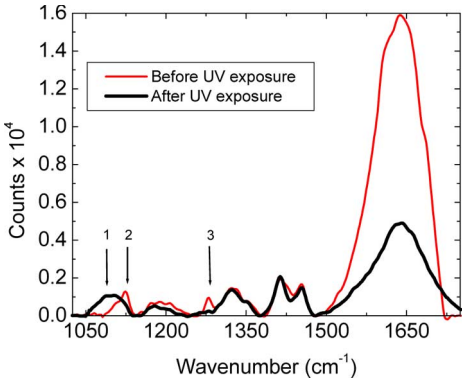

Fig. 11. Raman spectra obtained using an HC-PCF before and after UV exposure. The concentration of both solutions is approximately 10 mg of PAA per milliliter of water. The key modes. 1) 1092 cm^{-1}. 2) 1110 cm^{-1}. 3) 1279 cm^{-1}. The changes in the Raman spectra imply there are conformational and chemical changes that tend to enhance the final stability of the nanoparticle. A list of modes is given in the Appendix.

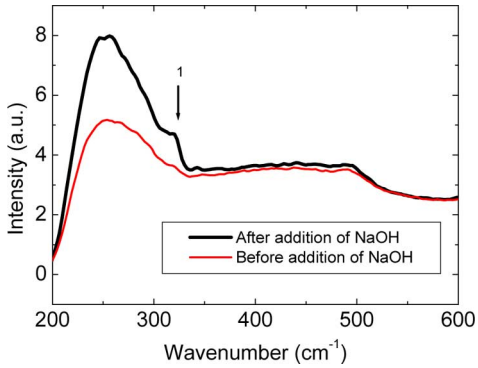

Fig. 12. Raman spectra comparing the changes before and after the addition of NaOH. The concentration of both solutions used was approximately 1 mg of solutes per milliliter of water. The appearance of the narrow mode 1) at 318 cm^{-1} is attributed to the creation of ZnO in the NP. This mode is observed from ZnO powder dissolved in water, as seen in Fig. 8.

Raman modes as compared to equivalent solution not exposed to UV radiation. Fig. 11 shows the Raman spectra of the UV irradiated and the nonirradiated solution.

An important change is the disappearance of the Raman mode centered at 1279 cm^{-1} after irradiation. This mode has been identified as C–O stretching and O–H bending modes [17]. In addition, after UV radiation, there is a shift to smaller wavenumbers accompanied by broadening for the modes centered around 1110 and 1092 cm^{-1}. These observed changes for the Raman modes suggest that exposure of the solution to UV-irradiation induces conformational and chemical changes in the polymer that enhances stability of the final NPs. Comparable spectra were obtained previously, where pump power $\sim$500 mW was used [17].

D. Step 3: Addition of Base and Induction of Crystallinity

The next step in the formation of ZnO is the addition of NaOH to form $Zn(OH)_2$ followed by hydrolysis to form ZnO. A new mode appears at 318 cm^{-1} with an FWHM of 13.91 cm^{-1}, as shown in Fig. 12. This mode is attributed to a second-order Raman mode of ZnO [33]. It should be noted that this is the same mode observed previously for ZnO powder in solution in

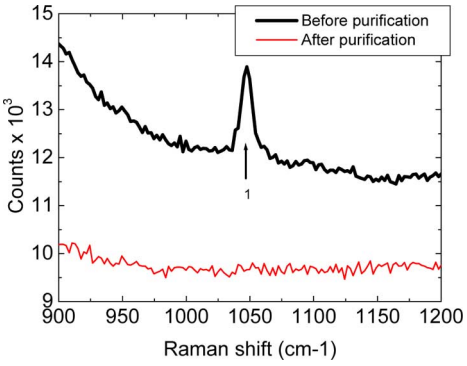

Fig. 13. Raman spectra of the ZnO NPs before and after purification. The solutions are 99% water by weight in both cases. The Raman mode 1) is centered at 1047 cm^{-1} and corresponds to symmetric stretching of the NO_3 species. The NO_3 species is eliminated by the purification process. This is corroborated in the lower spectrum with the disappearance of the relevant mode. A list of modes is given in the Appendix.

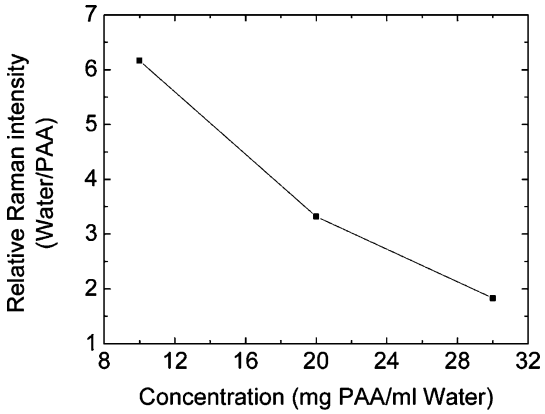

Fig. 14. Plot of the relative intensity of the water mode at 1650 cm^{-1} and that of the PAA mode at 1450 cm^{-1} versus the PAA concentration in solution. The correlation between both demonstrates how the ratio of the Raman modes can be used to obtain the PAA concentration in solution.

Fig. 8. This confirms the formation of ZnO in the NPs growth process. Other LO and TO modes of ZnO overlap with the dominant Raman signal generated from the silica fiber in the region between 300 and 500 cm^{-1}, and hence are not observed [33].

E. Step 4: Nanoparticle Purification

The last step in the synthesis process is to precipitate the ZnO NPs in order to eliminate any contamination from the remaining ions or polymer chains that did not aggregate. NPs are purified by precipitation with ethanol. The precipitate is then washed several times with 75% ethanol to remove any excess ions and polymer. After drying, the precipitate is then redispersed in deionized water. Comparison of the Raman spectra before and after the purification is shown in Fig. 13. The mode at 1047 cm^{-1} is a signature of the NO_3 species [35] that was introduced earlier in the synthesis process. This demonstrates that Raman spectroscopy in HC-PCF can effectively monitor the elimination of contaminants during synthesis.

F. Measuring the Concentration of PAA/Water Solutions

Measuring the concentration of PAA in water using Raman spectroscopy has also been explored. Three different solutions were prepared including 30, 20, and 10 mg of PAA per milliliter of water. By taking the ratio of the intensity of the water mode at 1640 cm^{-1} [34] to the intensity of the CH_2 deformation mode at 1450 cm^{-1} [17], a clear trend in this ratio with the PAA concentration is obtained, as shown in Fig. 14. This demonstrates the capability of the technique presented to also monitor the concentration of the solutions examined with sensitivity in the millimolar range.

G. Discussion

The Raman spectra plotted in Fig. 15 summarize the changes observed in the Raman spectra as the ZnO synthesis process progresses. These measurements were carried out using only 5.0 cm segments of HC-PCF. Moving to longer samples can accordingly increase the signal to noise ratio. The Raman modes obtained can also be used to examine the size distribution of the NPs, as has been demonstrated recently using Raman spectroscopy in a different material system [37]. As demonstrated here, information on impurity concentration as well as the concentration of the NPs can also be retrieved via amplitude ratios of Raman modes. The distinct advantages offered by the technique described here suggest that it can serve as an optimal candidate for *in situ* monitoring of NPs synthesis. Additionally, it is not limited by the index of refraction of the solution in which the NPs are fabricated. Other degrees of freedom such as the use of different pump powers and pump wavelengths may elucidate further on the properties of the NPs studied [37]. It must be emphasized that all these advantages do not limit themselves to the study of NPs, but can be equally valuable for biological samples, where the maximum allowable pump powers are naturally limited by the tolerance of the biological samples studied.

V. Conclusion

HC-PCFs were employed for enhancing the Raman signals obtained from dilute ZnO NPs in solution. By selectively filling the core of HC-PCF, substantial enhancement in the Raman signal was obtained. Raman modes pertinent to PAA, ZnO NPs, and its precursors were observed using record low pump power levels using this technique. Four different stages of ZnO NPs synthesis were studied. The concentration of ZnO was $<1\%$ by weight of the total mass of the system studied. Yet, the different synthesis stages could be differentiated, and the differences in the solution could be identified through the Raman modes obtained. This suggests that the technique presented could serve as an optimum means of *in situ* monitoring of NPs synthesis. It was also demonstrated that the NPs concentration in solution could be obtained with sensitivity in the millimolar range. This could be achieved by examining the ratios of the amplitudes of the Raman modes pertinent to water with respect to those of the polymer modes. The paper also demonstrated how Raman spectroscopy can be employed as an effective tool to monitor impurity concentration within the system.

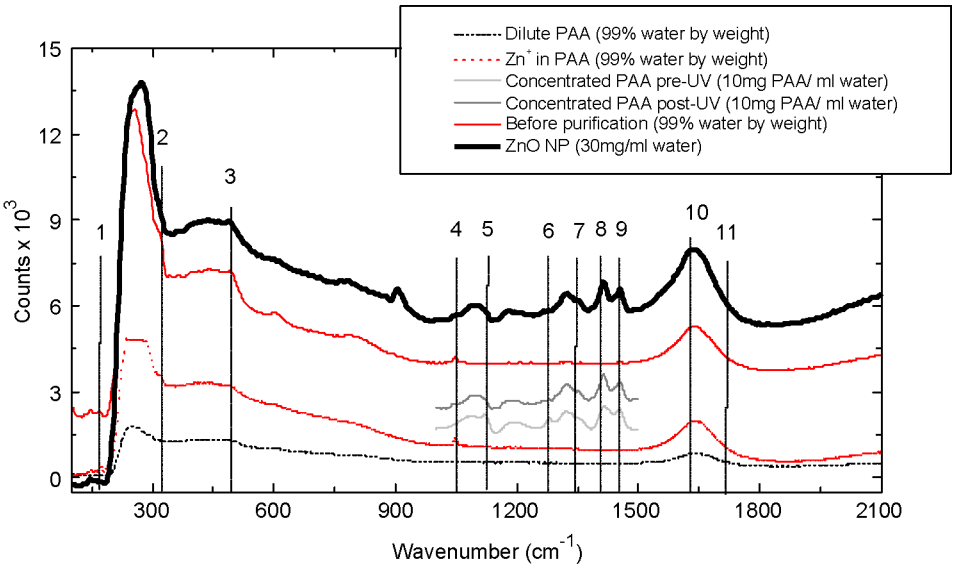

Fig. 15. Summary of Raman spectra obtained for different stages of ZnO NP synthesis. The vertical lines indicate the regions with important Raman modes, some of which change drastically during the different growth stages and some other that are static throughout fabrication. The modes shown here are as follows: 1) $Zn(NO_3)_2$ impurity mode at 173 cm^{-1}. 2) ZnO crystallinity mode at 318 cm^{-1}. 3) HC-PCF silica mode. 4) NO_3 impurity mode at 1046 cm^{-1}. 5) UV-sensitive polymeric mode at 1124 cm^{-1}. 6) UV-sensitive PAA mode at 1279 cm^{-1}. 7)–9) Standard PAA modes. 10) Water OH bending modes. 11) C=O mode at 1685 cm^{-1} (see the Appendix).

APPENDIX

TABLE I
RAMAN MODE DETAILS

Fig.	Material	Center (cm-1)	Width (cm-1)	Counts (a.u)	Assignment	Ref.
6	PAA (30mg/ml water)	908	24	1272	unidentified	-
		1052	31	251	CH_2 stretch	17
		1097	45	1076	C-CH_2 stretch	17
		1175	20	416	C-O stretch	17
		1199	28	315	C-O stretch	17
		1323	39	1294	CH_2 twisting	17
		1354	13	393	CH_2 twisting	17
		1414	24	1951	CH_2 deform	17
		1452	23	1414	CH_2 deform	17
		1590	92	1578	Water	34
		1644	71	3466	Water	34
		1685	64	389	C=O stretch	17
8	ZnO bulk	318	15	386	2^{nd} order	33
9	Water	1576	100	750	OH bending	34
		1640	78	2492	OH bending	34
		1695	83	752	OH bending	34
		2016	83	228	OH libration	34
		2094	100	545	OH libration	34
		2185	100	445	OH libration	34
		3234	222	7801	OH stretch	34
		3419	214	10335	OH stretch	34
		3552	183	3800	OH stretch	34
10	NO_3	1048	10	827	NO_3 stretch	35
		171	218	10.8	Zn-NO_3	38
11	Pre- UV	1110	24.8	691	C-CH_2 stretch	17
		1125	13.9	1018	Un-identified	-
		1279	10.	673	C-O and O-H	17
	Post-UV	1092	43.7	1062	C-CH_2 stretch	17
		1116	21	434	Un-identified	-
		1279	-	-	C-O and O-H	17
12	ZnO NPs	318	13.91	6667	2^{nd} order	33
13	NO_3	1048	10.51	1954	NO_3 stretch	35

REFERENCES

[1] V. I. Klimov, *Semiconductor, and Metal Nanocrystals: Synthesis and Electronic and Optical Properties*. New York: Marcel Dekker, 2004.

[2] Y. Yadong and P. Alivisatos, "Colloidal nanocrystal synthesis and the organic–inorganic interface," *Nature*, vol. 437, pp. 664–670, 2005.

[3] D. J. Milliron, I. Gur, and A. P. Alivisatos, "Hybrid organic—Nanocrystal solar cells," *MRS Bull.*, vol. 30, pp. 41–44, 2005.

[4] G. Konstantatos and E. H. Sargent, "PbS colloidal quantum dot photoconductive photodetectors: Transport, traps, and gain," *Appl. Phys. Lett.*, vol. 91, 173505, 2007.

[5] T. Neuberger, B. Schopf, H. Hofmann, M. Hofmann, and B. von Rechenberg, "Superparamagnetic nanoparticles for biomedical applications: Possibilities and limitations of a new drug delivery system," *J. Magn. Magn. Mater.*, vol. 293, pp. 483–496, 2005.

[6] W. J. Parak, D. Gerion, T. Pellegrino, D. Zanchet, C. Micheel, S. C. Williams, R. Boudreau, M. A. Le Gros, C. A. Larabell, and A. P. Alivisatos, "Biological applications of colloidal nanocrystals," *Nanotechnology*, vol. 14, pp. R15–R27, 2003.

[7] Y. H. Zheng, C. Q. Chen, Y. Y. Zhan, X. Y. Lin, Q. Zheng, K. M. Wei, J. F. Zhu, and Y. J. Zhu, "Luminescence and photocatalytic activity of ZnO nanocrystals: Correlation between structure and property," *Inorg. Chem.*, vol. 46, pp. 6675–6682, 2007.

[8] N. Toshima and T. Yonezawa, "Bimetallic nanoparticles—Novel materials for chemical and physical applications," *New J. Chem.*, vol. 22, pp. 1170–1201, 1998.

[9] J. M. Slaughter and C. M. Falco, "Advances in multilayer X-ray optics," *Nucl. Instrum. Methods Phys. Res. Sect. A: Accelerators*, vol. A319, pp. 163–169, 1992.

[10] G. Cao, *Nanostructures & Nanomaterials: Synthesis, Properties & Applications*. London, U.K.: Imperial College Press, 2004.

[11] G. Schmid, *Clusters and Colloids: From Theory to Applications*. New York: VCH, 1994.

[12] L. Ozawa, *Cathodoluminescence and Photoluminescence: Theories and Practical Applications*. Boca Raton, FL: CRC Press, 2007.

[13] D. A. Long, *The Raman Effect: A Unified Treatment of the Theory of Raman Scattering by Molecules*. New York: Wiley, 2002.

[14] G. Gouadec and P. Colomban, "Raman spectroscopy of nanostructures and nanosized materials," *J. Raman Spectrosc.*, vol. 38, pp. 598–603, 2007.

[15] M. A. Stroscio, *Phonons in Nanostructures*. New York: Cambridge Univ. Press, 2001.

[16] R. S. Krishnan and R. K. Shankar, "Raman effect: History of the discovery," *J. Raman Spectrosc.*, vol. 10, pp. 1–8, 1981.

[17] J. Dong, Y. Ozaki, and K. Nakashima, "Infrared, Raman, and near-infrared spectroscopic evidence for the coexistence of various hydrogen-bond forms in poly(acrylic acid)," *Macromolecules*, vol. 30, pp. 1111–1117, 1997.

[18] M. Moskovits, "Surface-enhanced spectroscopy," *Rev. Mod. Phys.*, vol. 57, pp. 783–826, 1985.

[19] K. Kneipp, M. Moskovits, and H. Kneipp, *Surface-Enhanced Raman Scattering: Physics and Applications*. New York: Springer-Verlag, 2006.
[20] F. S. Parker, *Applications of Infrared, Raman, and Resonance Raman Spectroscopy in Biochemistry*. New York: Plenum Press, 1983.
[21] J. X. Cheng and X. S. Xie, "Coherent anti-Stokes Raman scattering microscopy: Instrumentation, theory, and applications," *J. Phys. Chem. B*, vol. 108, pp. 827–840, 2004.
[22] R. Altkorn, I. Koev, and M. J. Pelletier, "Raman performance characteristics of Teflon(R)-AF 2400 liquid-core optical-fiber sample cells," *Appl. Spectrosc.*, vol. 53, pp. 1169–1176, 1999.
[23] R. Altkorn, M. D. Malinsky, R. P. Van Duyne, and I. Koev, "Intensity considerations in liquid core optical fiber Raman spectroscopy," *Appl. Spectrosc.*, vol. 55, pp. 373–381, 2001.
[24] P. Russell, "Photonic crystal fibers," *Science*, vol. 299, pp. 358–362, 2003.
[25] J. D. Joannopoulos, *Photonic Crystals: Molding the Flow of Light*. Princeton, NJ: Princeton Univ. Press, 1995.
[26] A. Bjarklev, *Photonic Crystal Fibers*. Boston, MA: Kluwer, 2003.
[27] C. M. Cordeiro, E. M. d. Santos, C. H. B. Cruz, and C. J. d. Matos, "Side access to the holes of photonic crystal fibers—New sensing possibilities," presented at the Opt. Fiber Sens., Cancun, Mexico, 2006, Paper ThE68.
[28] J. M. Fini, "Microstructure fibres for optical sensing in gases and liquids," *Meas. Sci. Technol.*, vol. 15, pp. 1120–1128, 2004.
[29] Thorlabs, "Data sheets for photonics crystal fibers."
[30] L. Xiao, W. Jin, M. Demokan, H. Ho, Y. Hoo, and C. Zhao, "Fabrication of selective injection microstructured optical fibers with a conventional fusion splicer," *Opt. Exp.*, vol. 13, pp. 9014–9022, 2005.
[31] Y. D. Shikhmurzaev, *Capillary Flows With Forming Interfaces*. Boca Raton, FL: CRC Press, 2008.
[32] D. Hollenbeck and C. D. Cantrell, "Multiple-vibrational-mode model for fiber-optic Raman gain spectrum and response function," *J. Opt. Soc. Amer. B, Opt. Phys.*, vol. 19, pp. 2886–2892, 2002.
[33] U. Ozgur, Y. I. Alivov, C. Liu, A. Teke, M. A. Reshchikov, S. Dogan, V. Avrutin, S. J. Cho, and H. Morkoc, "A comprehensive review of ZnO materials and devices," *J. Appl. Phys.*, vol. 98, pp. 0413011–041301-3, 2005.
[34] Z. Wang, A. Pakoulev, Y. Pang, and D. D. Dlott, "Vibrational substructure in the OH stretching transition of water and HOD," *J. Phys. Chem. A*, vol. 108, pp. 9054–9063, 2004.
[35] A. Wahab and S. Mahiuddin, "Isentropic compressibility, electrical conductivity, shear relaxation time, surface tension, and Raman spectra of aqueous zinc nitrate solutions," *J. Chem. Eng. Data*, vol. 49, pp. 126–132, 2004.
[36] R. D. Yang, S. Tripathy, Y. Li, and H.-J. Sue, "Photoluminescence and micro-Raman scattering in ZnO nanoparticles: The influence of acetate adsorption," *Chem. Phys. Lett.*, vol. 411, pp. 150–154, 2005.
[37] A. H. Nejadmalayeri, P. Scrutton, J. Mak, A. S. Helmy, P. R. Herman, J. Burghoff, S. Nolte, A. Tunnermann, and J. Kaspar, "Solid phase formation of silicon nanocrystals by bulk ultrafast laser–matter interaction," *Opt. Lett.*, vol. 32, pp. 3474–3476, 2007.
[38] S. Foley and M. Enescu, "A Raman spectroscopy and theoretical study of zinc–cysteine complexation," *Vib. Spectrosc.*, vol. 44, pp. 256–265, 2007.

Juan Irizar (S'08) received the B.Sc. degree in biomedical engineering in 2002 from the University of Toronto, Toronto, ON, Canada, where he is currently working toward the Master's degree.

His current research interests include Raman spectroscopy with photonic crystal fibers, biological spectroscopy with nuclear magnetic resonance, engineering cryobiology, and ocular fluid mechanics.

Jordan Dinglasan received the B.Sc. degree in chemistry from the University of the Philippines, Quezon City, Philippines, in 1997, and the M.Sc. and Ph.D. degrees from the University of Toronto, Toronto, ON, Canada, in 2001 and 2005, respectively.

He is the Co-Founder and the Development Scientist of Northern Nanotechnologies, Toronto. His current research interests include electrical properties in molecules in tunnel junctions and polyelectrolyte conformations in solution.

Jane Betty Goh received the B.S. degree in chemistry from the University of the Philippines, Quezon City, Philippines, in 1989, and the Ph.D. degree from Emory University, Atlanta, GA, all in chemistry, in 1997.

Altaf Khetani received the Engineering degree in electronics and communication from Osmania University, Hyderabad, India, in 2005. He is currently working toward the M.A.Sc. degree in electrical engineering at the University of Ottawa, Ottawa, ON, Canada.

His current research interests include photonic crystal fiber for biosensing application.

Hanan Anis received the B.Sc. degree from Ain-Shams University, Cairo, Egypt, in 1987, the M.A.Sc. degree in 1999, and the Ph.D. degree in 1996 from the University of Toronto, Toronto, ON, Canada, both in electrical and computer engineering.

Since July 2004, she has been an Associate Professor in the School of Information Technology (SITE), University of Ottawa, Ottawa, ON. Prior to that, she was the Co-Founder and a Chief Technology Officer at Ceyba. From 1994 to 2000, she was with Nortel Networks, where she was engaged in photonics, ranging from device physics to optical networking. She is the author or coauthor of several papers published in journals and conferences, and holds several patents. Her current research interests include soliton generation and detection, nonlinear propagation, tunable lasers, agile all-optical networks, and high-end transmission systems.

Dr. Anis was the recipient of the Nortel's 1998 Innovation Award for her contribution on wavelength-locked lasers.

Darren Anderson received the B.Sc., M.Sc., and Ph.D. degrees in physical chemistry from the University of Toronto, Toronto, ON, Canada, in 2001, 2002, and 2006, respectively.

Since 2006, he is with Northern Nanotechnologies, Toronto, and is currently a Chief Technology Officer. He is the author or coauthor of several papers published in journals and conferences. His current research interests include synthesis and use of gold and silver nanoparticles, use of nanostructures to guide surface plasmon propagation in gold surfaces, and the interactions of complex biological molecules to form large superstructures.

Dr. Anderson was the recipient of the Natural Sciences and Engineering Research Council (NSERC) Doctoral Fellowship in 2004.

Cynthia Goh received the B.S. degree in chemistry from the University of the Philippines, Quezon City, Philippines, in 1980, and the Ph.D. degree from the University of California, Los Angeles (UCLA), all in chemistry, in 1985.

Since 1990, she has been at the University of Toronto, Toronto, ON, Canada, where she is currently a Full Professor in the Department of Chemistry and an Associate Director at the Institute for Optical Sciences.

A. S. Helmy (M'99–SM'06) received the B.Sc. degree in electronics and telecommunications engineering from Cairo University, Cairo, Egypt, in 1993, and the M.Sc. and Ph.D. degrees in photonic fabrication technologies from the University of Glasgow, Glasgow, U.K., in 1994 and 1999, respectively.

He was in the R&D Division, Agilent Technologies Photonic Devices, U.K., where he was engaged in developing distributed feedback lasers, monolithically integrated lasers, modulators, and amplifiers in InP-based semiconductors. He was also engaged in developing high-powered submarine-class 980-nm InGaAs pump lasers. He is currently an Assistant Professor in the Department of Electrical and Computer Engineering, University of Toronto, Toronto, ON, Canada. His current research interests include photonic device physics and characterization techniques, with emphasis on nonlinear optics in III–V semiconductors, applied optical spectroscopy in III–V optoelectronic devices and materials, and III–V fabrication and monolithic integration techniques.

Dr. Helmy is a member of the Optical Society of America.